Contents lists available at ScienceDirect

Transactions of Nonferrous Metals Society of China

36(2026) 855−871

www.tnmsc.cn

A machine learning strategy for rapid design of preparation parameters in zero-sample complex alloy

Hui-qiang MA [a], Hong-tao ZHANG [a,b,c,**], Hua-dong FU [a,b,c,d], Jing-tai SUN [a], Jian-xin XIE [a,b,c,d,*]

[a] Beijing Advanced Innovation Center for Materials Genome Engineering, University of Science and Technology Beijing, Beijing 100083, China;

[b] Key Laboratory for Advanced Materials Processing (MOE), University of Science and Technology Beijing, Beijing 100083, China;

[c] Beijing Laboratory of Metallic Materials and Processing for Modern Transportation, University of Science and Technology Beijing, Beijing 100083, China;

[d] Institute of Materials Intelligent Technology, Liaoning Academy of Materials, Shenyang 110004, China

Abstract: To address the zero-sample challenge in preparation parameter design for newly developed alloys, a novel machine learning strategy that integrates basic dataset construction with Bayesian optimization, was proposed. The impact of basic sample dataset construction methods, optimization benchmarks and multi-objective utility functions on Bayesian optimization was investigated. It was found that the combination of orthogonal design, linear benchmark, and shifted multiplicative utility function exhibits the best optimization performance. The strategy was then applied to a new Cu−Ni−Co−Si alloy with ultra-low Co content (0.7 wt.% Co), previously designed by our research team. Rapid optimization of six preparation parameters in the two-stage deformation and aging process of the zero-sample alloy was achieved through only 23 experiments. The measured ultimate tensile strength and electrical conductivity of the new alloy were 878 MPa and 44.0%(IACS), respectively, reaching the comprehensive performance level of the Cu−Ni−Co−Si alloy (C70350 alloy) containing 1.0−2.0 wt.% Co.

Keywords: Cu−Ni−Co−Si alloy; preparation parameters; machine learning; Bayesian optimization

1 Introduction

High-strength, high-conductivity copper alloys with excellent mechanical and electrical properties are critical materials for the manufacture of products in the fields of electronic information and communication [1−4]. Among these, precipitation-strengthened Cu−Ni−Si alloys, particularly Cu−Ni−Co−Si alloys, offer advantages such as high strength, high conductivity, and non-magnetic properties. As a result, they are widely used as lead-frame materials for integrated circuits [5−7]. The demand for high-performance, cost-effective lead-frame materials is a key driver for the future development of advanced integrated circuits. Therefore, the development of new Cu−Ni−Co−Si alloys with low Co content and high overall performance represents a crucial direction for the advancement of next-generation alloys.

The composition and preparation parameter design are critical approaches to enhance the comprehensive performance of copper alloys, particularly for newly designed alloys, which require well-optimized preparation parameters to achieve high overall performance [8−11]. The precipitation-

Corresponding author: *Jian-xin XIE, Tel: +86-10-62332254, E-mail: jxxie@mater.ustb.edu.cn;
**Hong-tao ZHANG, Tel: +86-10-62333999, E-mail: zht@ustb.edu.cn

https://doi.org/10.1016/S1003-6326(25)67002-6
Received 3 June 2024; accepted 25 March 2025

strengthened copper alloys often involve complex preparation processes, numerous parameters, and intricate interactions between these parameters, making the design of preparation parameters challenging. In recent years, rapidly advancing data-driven methods have revolutionized material research and development, with machine learning playing a key role in numerous applications. These techniques have significantly improved the efficiency of material preparation parameter design [12−15]. For example, NGUYEN et al [16] constructed a deep learning-based optimization system to accelerate the selection of selective laser melting parameters for Ti−6Al−4V. TAMURA et al [17] employed a Bayesian optimization method to design preparation parameters for powder production through gas atomization of Ni−Co-based superalloy, achieving a 72% reduction in cost while improving powder yield.

The design of preparation parameters often faces the challenge of limited or even zero-sample data, making rapid design using machine learning methods particularly difficult. Bayesian optimization addresses this issue by iteratively supplementing key experimental data, thereby significantly reducing the experimental workload. This approach has been successfully applied to the design of preparation parameters for a variety of materials. For example, CHEN et al [18] proposed a machine learning-assisted strategy to optimize the two-stage aging preparation parameters via an iterative approach, resulting in a 27% increase in strength and 13.5% improvement in plasticity for cast ZE62 magnesium alloy. ZHANG et al [19] utilized Bayesian optimization to design preparation parameters for copper alloys, successfully determining three parameters for the secondary deformation−aging process with only five iterative experiments, which led to a significant enhancement in comprehensive performance of the alloy.

However, for newly designed alloys, the rapid design of preparation parameters using machine learning methods such as Bayesian optimization often encounters the challenge of zero-sample data. For example, in the development of high-performance, low-cost lead-frame materials for high-end integrated circuits, the authors' research group has designed a new Cu−Ni−Co−Si alloy. The two-stage deformation−aging process is a critical step in the preparation of the alloy, involving six alloy preparation parameters, which presents a large experimental trial-and-error space, and these six preparation parameters have zero-sample data. To address the challenges posed by zero-sample data, in this paper, we proposed a preparation parameter design strategy that combines basic dataset construction with Bayesian optimization. The study clarifies the influence of basic sample dataset construction methods, optimization benchmarks, and multi-objective utility functions on the effectiveness of Bayesian optimization, and successfully achieves the rapid design of two-stage deformation−aging preparation parameters for the new Cu−Ni−Co−Si alloy with ultra-low Co content. This work offers a novel strategy for the efficient design of preparation parameters for complex alloys.

2 Strategy and methods

2.1 Design strategy

The research process was as fallows: construction of basic sample dataset → benchmark design → multi-objective utility function design→ Bayesian optimization and experiment iteration. Initially, a simulation function was employed to explore the construction of the basic sample dataset and the design of the benchmark. Subsequently, experimental iterations of copper alloy preparation parameters were conducted to compare the optimization effects of different multi-objective utility functions, as shown in Fig. 1.

The space of the six preparation parameters in the two-stage deformation−aging process for copper alloys is large, and the combinations of basic sample dataset construction methods and optimization benchmarks can reach up to 12. As a result, using experimental comparisons to identify the appropriate methods for constructing the basic sample dataset and selecting the benchmark would be labor-intensive and difficult to achieve. To address this issue, we evaluated the impact of different basic sample dataset construction methods and benchmarks on optimization efficiency through a simulation function.

The primary strengthening mechanism of Cu−Ni−Co−Si alloy is precipitation strengthening, which is commonly calculated using the Orowan−Ashby equation [20,21], as shown in Eq. (1). This formula contains six independent variables, which align with the number of two-stage deformation−

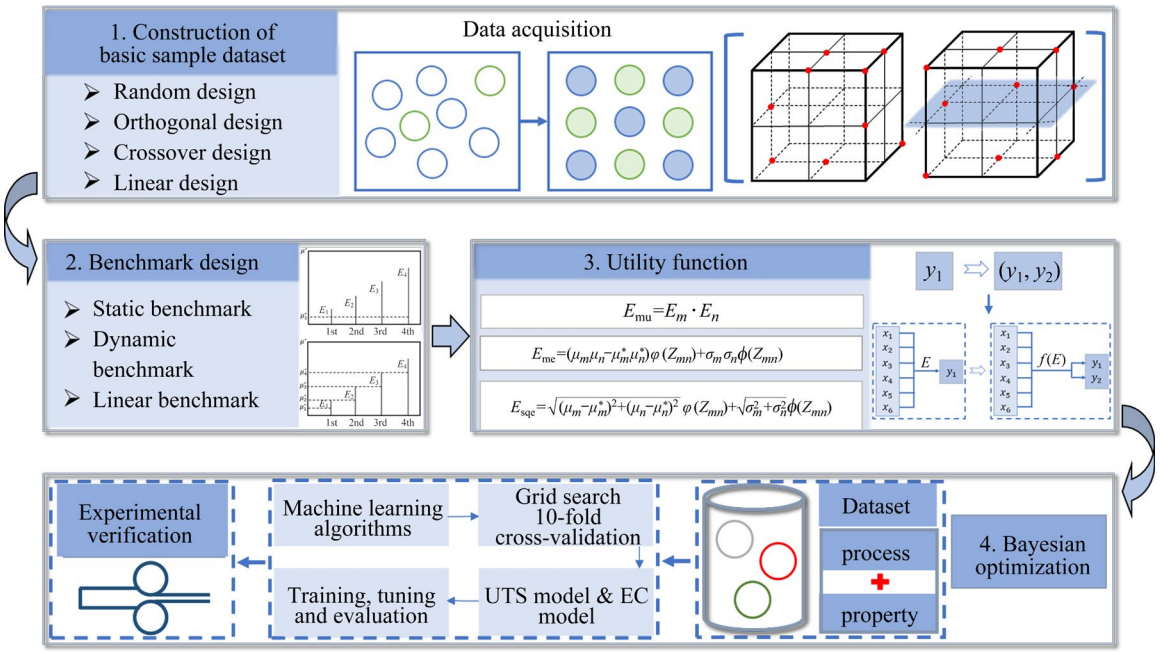

Fig. 1 Preparation parameter design strategy integrating basic dataset construction with Bayesian optimization

aging parameters in the copper alloys in this study. Therefore, we employed this equation as the simulation function (dimensionless) in the Bayesian optimization process.

$$\Delta\sigma_{\text{Orowan}}=\frac{0.81MGb}{2\pi(1-\nu)^{1/2}}\frac{\ln(d_{\text{p}}/b)}{d_{\text{p}}\sqrt{\frac{3\pi}{8f_{\text{v}}}}-d_{\text{p}}} \quad (1)$$

where $\Delta\sigma_{\text{Orowan}}$ is the precipitation strengthening, M is the Taylor factor, G is the matrix shear modulus, b is the magnitude of Burgers vector, ν is the Poisson ratio, d_{p} is the average diameter of the precipitate phases, and f_{v} is the volume fraction of the precipitate phases.

The $\Delta\sigma_{\text{Orowan}}$ in Eq. (1) is considered as the target variable, and M, G, b, ν, d_{p}, and f_{v} as the input variables. The corresponding value ranges are defined according to the possible values of each parameter, and the parameter candidate space for the simulation function is designed as shown in Table 1, containing 1331000 parameter combinations.

Table 1 Candidate space for simulation function parameters (Dimensionless)

Candidate space	M	G	b	ν	d_{p}	f_{v}
Value range	1−10	10000−100000	0−1	0−1	1−10	0−0.01
Step	1	10000	0.1	0.1	1	0.001

(1) Basic sample dataset construction method

In order to obtain suitable methods for constructing basic sample datasets, four commonly used approaches were compared and studied: orthogonal design, random design, crossover design, and linear design. Among these, the orthogonal design generates 18 datasets with 6 factors, each at three levels. To maintain consistency in sample size, the other three methods also generate 18 datasets. The random design method involves generating 18 datasets randomly. The crossover design method first generates 9 datasets using random design, and then designs another 9 datasets based on symmetrical positions. The linear design method initially generates 9 datasets by randomly designing the first three parameters, selects a set of high-performance parameters, and then generates the remaining 9 datasets by randomly designing the last three parameters, resulting in a total of 18 datasets.

(2) Benchmark design

Bayesian optimization typically involves two types of optimization benchmarks: static and dynamic. In this paper, a linear benchmark was proposed based on the characteristic of the gradual increase in the comprehensive performance of copper alloys, and the impact of three types of benchmarks on the design effect was compared. The static benchmark selects the highest value of the target parameter in the basic sample dataset as the

reference for subsequent design and iteration, with the benchmark remaining fixed throughout the process. The dynamic benchmark, on the other hand, uses the highest value of the target parameter in the current dataset, which can change as the iterations progress, causing the benchmark to adjust accordingly. The linear benchmark takes the highest value of the target parameter in the basic sample dataset as a reference and increases it proportionally. For example, if the highest value of the target parameter in the basic sample dataset is 100, and a 20% linear scale is applied, the benchmark for the first three iterations will be 20, 40, and 60.

Subsequently, Bayesian optimization design and iteration were performed using the function in Eq. (1) to compare the effects of the four sample dataset construction methods and three benchmarks on the iteration outcome. This comparison aims to identify the most suitable sample dataset construction method and optimization benchmark. The Bayesian optimization process employed the utility function (E) shown in Eq. (2) for the design of each parameter.

$$E=\sigma[\varphi(Z)+Z\phi(Z)] \tag{2}$$

where σ is the standard deviation of model prediction; $\varphi(Z)$ and $\phi(Z)$ are the standard normal density and distribution functions, respectively (Integral in $(Z, +\infty)$), $Z=(\mu-\mu^*)/\sigma$ (μ is the predicted property; μ^* is the optimization benchmark).

(3) Multi-objective utility function design

In order to explore the form of a targeted multi-objective utility function for alloy deformation−aging preparation parameters, this study designed several multi-objective utility functions based on the commonly used utility function expected improvement (E). These utility functions are tailored to meet the multi-objective needs of copper alloys in enhancing both mechanical and electrical properties, as well as addressing the mutual constraints between these properties. For two variables Y_1 and Y_2 exhibiting an inverse relationship, the product $|Y_1|\cdot|Y_2|$ can be used to represent comprehensive performance. Additionally, statistical methods such as $Y_1\cdot Y_2$ and $\sqrt{Y_1^2+Y_2^2}$ are commonly applied. The advantage of these two methods over $|Y_1|\cdot|Y_2|$ is that they take into account the correlation between Y_1 and Y_2.

Building on these concepts, three multi-objective utility functions E_{mu} (Numerical multiplicative utility function), E_{me} (Linear multiplicative utility function), and E_{sqe} (Shifted multiplicative utility function) were designed in this paper, as shown in Eq. (3) to Eq. (5), respectively. E_{mu} [22] involves calculating the utility function for each objective separately and then combining them. The process is as follows: first, calculate the utility function E for the variables m and n individually, then multiply them to obtain the combined utility function. E_{me} converts the multi-objective utility function into a binary joint utility function in single-objective form, and the specific process involves multiplying the separate variables m and n to get the variable mn, and then computing the utility function E on the variable mn. E_{sqe} combines the two objectives using a distance formula. This involves replacing the mean and variance in E_{me} according to the distance formula.

$$E_{\mathrm{mu}}=E_m\cdot E_n=[(\mu_m-\mu_m^*)\varphi(Z_m)+\sigma_m\phi(Z_m)]\cdot [(\mu_n-\mu_n^*)\varphi(Z_n)+\sigma_n\phi(Z_n)] \tag{3}$$

$$E_{\mathrm{me}}=(\mu_m\mu_n-\mu_m^*\mu_n^*)\varphi(Z_{mn})+\sigma_m\sigma_n\phi(Z_{mn}) \tag{4}$$

$$E_{\mathrm{sqe}}=\sqrt{(\mu_m-\mu_m^*)^2+(\mu_n-\mu_n^*)^2}\,\varphi(Z_{mn})+\sqrt{\sigma_m{}^2+\sigma_n{}^2}\,\phi(Z_{mn}) \tag{5}$$

where $Z_m=\dfrac{\mu_m-\mu_m^*}{\sigma_m}$, $Z_n=\dfrac{\mu_n-\mu_n^*}{\sigma_n}$, $Z_{mn}=Z_m\cdot Z_n=\dfrac{\mu_m-\mu_m^*}{\sigma_m}\cdot\dfrac{\mu_n-\mu_n^*}{\sigma_n}$, $\varphi(Z_m)$, $\varphi(Z_n)$, $\phi(Z_m)$, and $\phi(Z_n)$ represent the standard normal density function value and the cumulative distribution function value of variables m and n, respectively. Assuming that variables m and n are independent of each other, $\varphi(Z_{mn})$ and $\phi(Z_{mn})$ represent the bivariate standard normal density function value and the bivariate cumulative distribution function value.

The three multi-objective utility functions constructed above were applied to the design and optimization of the two-stage deformation−aging process parameters of Cu−Ni−Co−Si alloy. The optimization effects of the three utility functions were compared.

(4) Bayesian optimization and experimental iteration of preparation parameters for copper alloys

The Bayesian optimization method has the characteristics of fewer iterations and strong global search ability [23]. Its core components include three aspects: machine learning model construction, utility function calculation, and experimental verification and iteration. In this study, the machine learning model was constructed using the basic sample data

obtained from orthogonal experiments. The utility function is a multi-objective utility function derived from the single-objective utility function E, designed to meet multi-objective performance requirements. The appropriate process parameters were then recommended based on the utility function, followed by experimental verification and feedback iteration.

In the first step, the basic sample dataset was constructed using the method obtained from the simulation screening. Based on the range of suitable preparation parameters for Cu−Ni−Co−Si system alloys reported in Refs. [24,25], the candidate space for experimental parameters was designed, as shown in Table 2, with a total of 313600 datasets. The basic sample dataset was then constructed by specifying the following experimental parameters: primary cold rolling deformation (CR_1) of 60%, 70%, and 80%; primary aging temperatures (T_1) of 450, 475, and 500 °C; primary aging time (t_1) of 1, 3, and 5 h; secondary cold rolling deformation (CR_2) of 60%, 70%, and 80%; secondary aging temperatures (T_2) of 450, 475, and 500 °C; secondary aging time (t_2) of 1, 3, and 5 h. The corresponding ultimate tensile strength (UTS) and electrical conductivity (EC) for the selected preparation parameters were experimentally tested. This results in the creation of a basic sample dataset consisting of the following variables: CR_1, T_1, t_1, CR_2, T_2, and t_2; the corresponding UTS and EC values.

In the second step, the machine learning model was constructed. To prevent overfitting, a combination of algorithm selection and cross-validation was employed. This approach ensures a reasonable match between the data and the algorithms, followed by the optimization of model parameters through ten-fold cross-validation. Firstly, we compared the modeling performance of several algorithms, including support vector regression (SVR), Bagging, decision tree regression (DT), k-nearest neighbors (KNN), and Gaussian process regression (GPR), etc, and selected the algorithms that yield the lowest prediction error. Next, two models were established: the "preparation parameters – UTS" model (referred to as the UTS model) and the "preparation parameters – EC" model (referred to as the EC model), with the six preparation parameters as inputs and UTS and EC as outputs, respectively. During the modeling process for both the UTS and EC models, ten-fold cross-validation was used to evaluate the mean absolute error (M_E) and optimize the model hyperparameters, as shown in Eq. (6):

$$M_E=\frac{1}{n}\frac{\left|P_{pre}-P_{exp}\right|}{P_{exp}}\times 100\% \tag{6}$$

where n is the sample size; P_{pre} and P_{exp} are the predicted and experimental values of the target property, respectively.

In the third step, Bayesian optimization was employed to design the preparation parameters. Following the methods outlined in Refs. [22,26,27], resampling modeling was used to obtain prediction values and their associated uncertainties, facilitating the calculation of the utility function. The training set data were resampled 1000 times, with 90% of the sample data randomly selected each time to establish the UTS and EC models. The mean and standard deviations of the predicted properties from the 1000 models were then used to compute the multi-objective utility functions E_{mu}, E_{me}, and E_{sqe} for each preparation parameter combination in the candidate space. The preparation parameter combinations corresponding to the maximum values of these utility functions were selected for experimental validation.

In the fourth step, experimental validation and feedback iteration were conducted. Experimental validation was carried out on the preparation parameters designed through Bayesian optimization to test the properties of the alloy specimens. The experimental parameters and corresponding property data from the tests were incorporated into the sample dataset, and the model was updated for the next round of Bayesian optimization in the preparation parameter design process. This feedback−iteration cycle continues until the comprehensive performance of the alloy begins to degrade.

Table 2 Experimental parameter candidate space

Candidate space	CR_1/%	T_1/°C	t_1/h	CR_2/%	T_2/°C	t_2/h
Value range	50−90	400−550	0.5−8	50−90	400−550	0.5−8
Step	10	25	0.5	10	25	0.5

2.2 Experimental methods

A new Cu−Ni−Co−Si alloy with ultra-low Co content with target properties of UTS (850 MPa) and EC (45%(IACS)) was previously designed using the machine-learning design method proposed by ZHANG et al [22]. The Co content was restricted to no more than 0.7 wt.%. The target properties of UTS (850 MPa) and EC (45%(IACS)) were selected with reference to the properties of the commercial high-end lead-frame material C70350. The Cu−Ni−Co−Si alloy was prepared by medium-frequency vacuum induction melting, and the designed and measured compositions are shown in Table 3. Drawing from industrial production experience, the alloy preparation process was as follows: casting → homogenization at 800 °C for 4 h → hot rolling with 67% reduction at 800 °C (from a thickness of 30 mm to 10 mm) → solid solution treatment at 960 °C for 1 h followed by water quenching. The prepared specimens were then used for studies on primary deformation−aging and secondary deformation−aging.

Table 3 Designed and measured copper alloy compositions (wt.%)

Alloy	Cu	Ni	Co	Si	Mg	Cr
Designed	Bal.	2.1	0.7	0.7	0.15	0.1
Measured	Bal.	2.06	0.68	0.79	0.15	0.11

Multi-stage deformation−aging treatment was carried out using the preparation parameters designed by Bayesian optimization with the following experimental method. Tensile specimens were prepared in accordance with the GB/T 228.1—2010 standard. The mechanical properties of the alloy specimens were tested using an MTS universal material testing machine, with a tensile chuck displacement rate of 1 mm/min. Three specimens were prepared for each aging condition, and the mechanical property test results were averaged. The specimens measuring 80 mm (length) × 2 mm (width) were cut, and the electrical resistance of the alloy was measured using an Applent AT−510Pro DC resistance tester. The EC was then calculated, with three specimens for each aging condition, and the results were averaged. The specimens were prepared using a Gantan691 dual-mill precision ion polishing system, and the microstructure was observed using a JEM2100 transmission electron microscope (TEM).

3 Results

3.1 Basic sample dataset construction and benchmark design

A comparison of the basic sample dataset construction methods was conducted using a simulation function, with 18 datasets collected for each method. The distributions of the sample datasets are shown in Fig. 2.

Bayesian optimization was then performed for each of the four basic sample dataset construction methods, paired with the three benchmarks, resulting in a total of 12 combinations. For each combination, 10 iterations of the Bayesian optimization process were carried out, and the results are presented in Fig. 3.

When comparing the sample dataset construction methods, it is observed that the orthogonal design consistently improves its performance during the iteration process with minimal fluctuation, while also achieving the highest maximum value in the iterations. This indicates that orthogonal design provides more reliable sample data for machine learning. Regarding the benchmarks, the iteration maximum value of the linear optimization benchmark reaches its highest value in both the orthogonal design and the linear design of the sample datasets, suggesting that the linear optimization benchmark is particularly suitable for these two designs. In the random design and crossover design, the iteration maximum value of the linear optimization benchmark is second only to that of the static optimization benchmark, indicating that the linear optimization benchmark also performs well in these two designs.

Figure 4 illustrates the impact of basic sample dataset construction methods and optimization benchmarks on the optimization. Based on the results of both the basic sample dataset construction and the optimization benchmark design, it can be concluded that the combination of orthogonal experimental design and linear optimization benchmark is the most effective approach for basic sample dataset construction and benchmark design. Therefore, in the subsequent work of this paper, we adopted the combination of orthogonal experimental design and linear optimization benchmark for the copper alloy preparation parameter design.

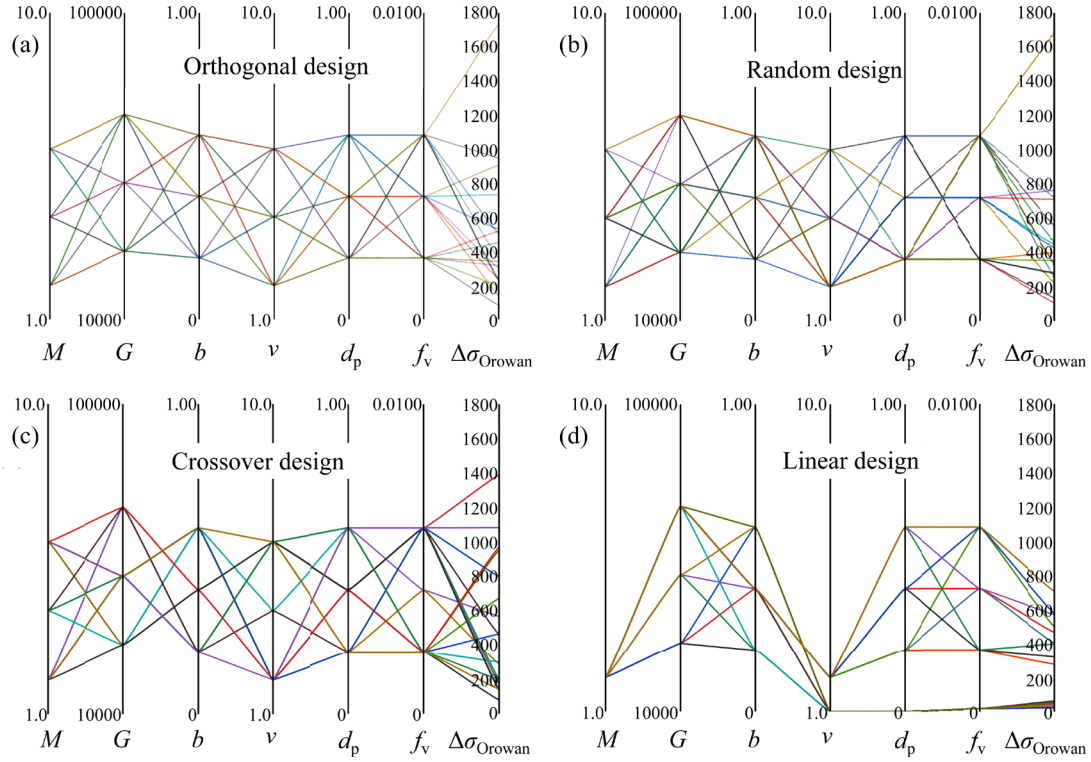

Fig. 2 Schematic diagrams of basic sample dataset (variables shown in this figure are dimensionless): (a) Orthogonal design; (b) Random design; (c) Crossover design; (d) Linear design

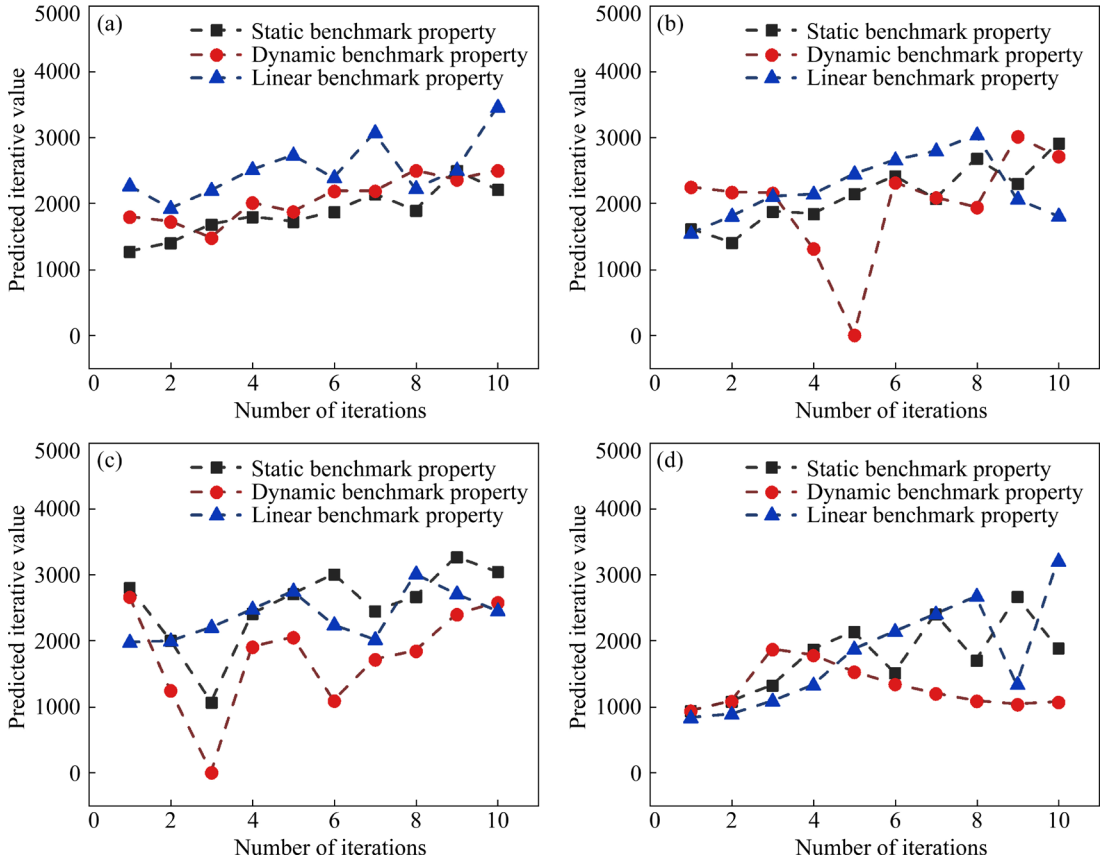

Fig. 3 Iterative optimization of simulation function: (a) Orthogonal design; (b) Random design; (c) Crossover design; (d) Linear design

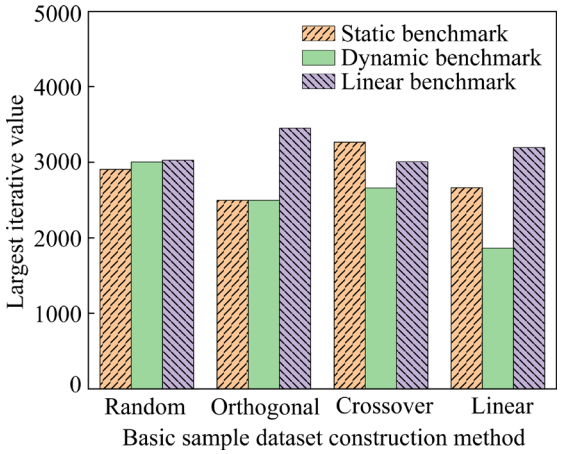

Fig. 4 Impact of basic sample dataset construction methods and benchmarks on optimization

3.2 Multi-objective utility functions and experimental validation

Orthogonal design was employed to collect sample data for the two-stage cold rolling and aging process of copper alloys. The parameters are defined as follows: CR_1 of 60%, 70%, and 80%; T_1 of 450, 475, and 500 °C; t_1 of 1, 3, and 5 h; CR_2 of 60%, 70%, and 80%; T_2 of 450, 475, and 500 °C; t_2 of 1, 3, and 5 h. The sample data collected are shown in Fig. 5(a). After undergoing the two-stage cold rolling and aging treatment, the UTS is found to range from 680 to 970 MPa, and the EC ranges from 32%(IACS) to 47%(IACS).

To select an appropriate machine learning algorithm and avoid overfitting, a ten-fold cross-validation method was used to compare the modeling performance of several algorithms, including SVR, Bagging, DT, KNN, and GPR, as shown in Figs. 5(c) and (d). As observed from the figures, the SVR algorithm yields the lowest error for both the UTS and EC models. Therefore, the SVR algorithm was selected for subsequent modeling and design.

The evaluation results (model errors) for the SVR-based modeling of 1000 samples from the basic sample dataset are presented in Fig. 5(b). The bars in the figure represent the mean and standard deviation of the errors for the 1000 models, while the gray area shows the error distribution of the validation set for

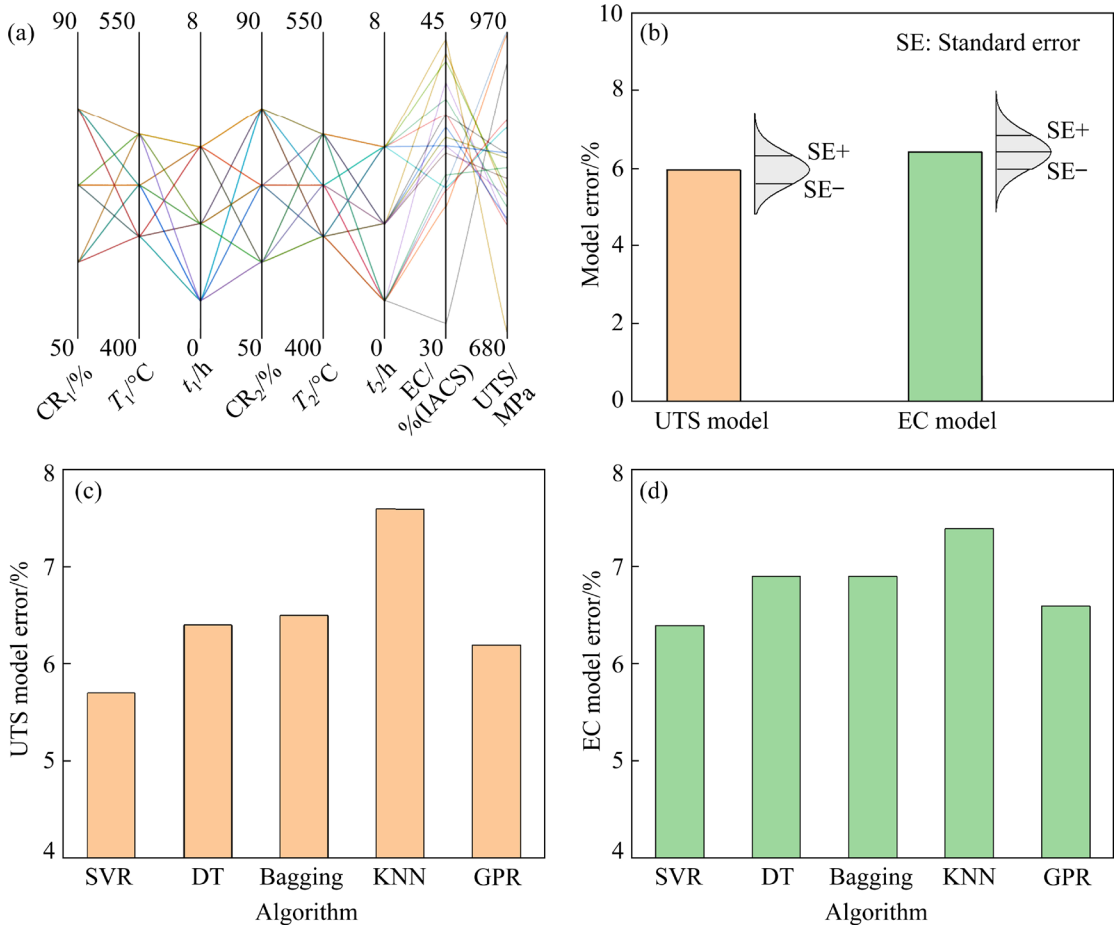

Fig. 5 Sample data and machine learning modeling: (a) Schematic diagram showing distribution of basic sample data; (b) Errors of 1000 UTS models and 1000 EC models based on SVR; (c) UTS model error; (d) EC model error

the 1000 models. The error for the UTS model is (5.9±0.4)%, and for the EC model, it is (6.4±0.5)%.

The multi-objective utility functions E_{mu}, E_{me}, and E_{sqe} were used to design the preparation parameters, followed by experimental validation and iteration. The results are presented in Table 4.

For E_{mu}, as the iterations progress, the primary aging time of the alloy increases from 6.5 to 8.0 h, while the secondary aging time is continuously adjusted. After three iterations, the comprehensive performance of the alloy reaches its peak, with a UTS of 877 MPa and an EC of 43.8%(IACS). The alloy performance begins to decline after the fourth iteration. For E_{me}, the five variables, i.e. primary cold rolling deformation, primary aging temperature and time, secondary aging temperature and time, are adjusted. After four iterations, the alloy achieves its highest performance, with a UTS of 868 MPa and an EC of 44.2%(IACS). After the fifth iteration, the alloy performance starts to decrease, and the iteration process is stopped. For E_{sqe}, after three iterations, the alloy reaches its highest performance with a UTS of 878 MPa and an EC of 44.0%(IACS). The alloy performance begins to decrease after the fourth iteration.

The properties of each sample in the basic sample dataset, along with the measured properties of the alloy specimens designed in each iteration, are plotted in Fig. 6. As shown in the plots, the optimal alloy performance during the corresponding experimental iterations of the three utility functions surpasses the best values in the basic sample data. The product values of UTS and EC obtained for each iteration of the three multi-objective utility functions are presented in Fig. 6(d). Using the product of UTS and EC as a basis for evaluating the alloy's comprehensive performance, it is evident that the highest performance is achieved in the third iteration of the multi-objective utility function E_{sqe}.

For the two-stage deformation and aging of copper alloy, a comparison of the iterative effects and the number of iterations for each multi-objective utility function reveals that the iterative efficiency of E_{sqe} is the highest, and the alloy performance after iteration is the best. It is worth noting that further iterations could potentially enhance the alloy's overall performance. However, due to the high cost of experiments and the need for rapid design, only five iterations were conducted.

Table 4 Iteration design results with multi-objective utility functions

Multi-objective utility function	Iteration order	CR_1/%	T_1/°C	t_1/h	CR_2/%	T_2/°C	t_2/h	UTS*/MPa	EC*/%(IACS)
E_{mu}	1st	60	500	6.5	60	400	3.0	916	41.1
	2nd	60	500	8.0	60	400	4.5	889	42.7
	3rd	60	500	8.0	60	400	5.0	877	43.8
	4th	60	500	8.0	60	400	4.0	870	43.1
	5th	60	500	8.0	60	400	3.5	844	42.6
E_{me}	1st	60	500	6.5	60	400	3.5	903	41.0
	2nd	60	500	7.0	60	400	5.5	898	41.9
	3rd	70	475	8.0	70	400	6.5	895	42.6
	4th	70	475	8.0	70	400	8.0	868	44.2
	5th	70	475	8.0	70	400	7.5	885	41.5
E_{sqe}	1st	50	550	7.0	70	400	8.0	797	44.3
	2nd	60	550	5.0	70	425	5.5	723	46.1
	3rd	60	500	6.0	70	425	6.0	878	44.0
	4th	70	450	6.5	70	400	5.0	922	40.3
	5th	70	450	6.0	70	400	6.0	900	39.1

* UTS and EC are experimental test results

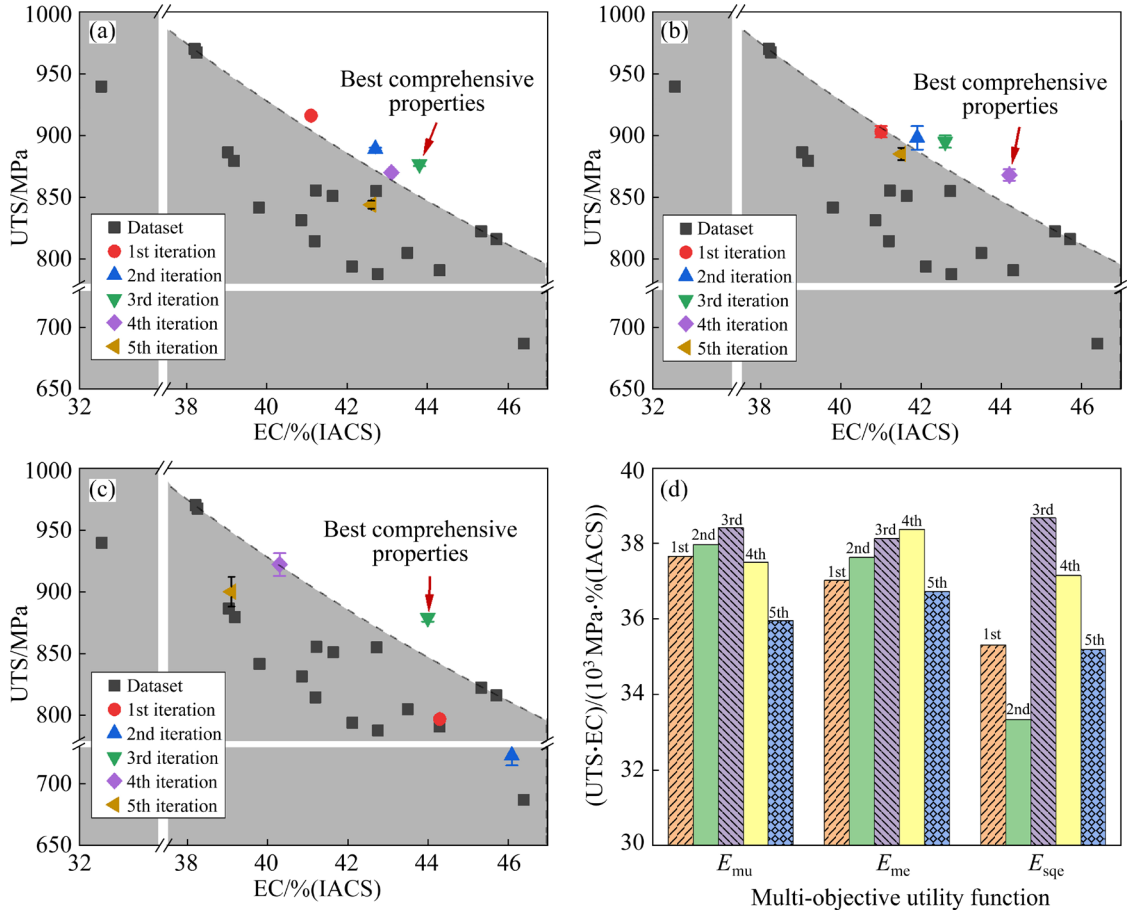

Fig. 6 Bayesian optimization iteration results using multi-objective functions: (a) E_{mu}; (b) E_{me}; (c) E_{sqe}; (d) UTS·EC

4 Discussion

4.1 Advantages of design strategy combining basic dataset construction and Bayesian optimization

The candidate space of the experimental parameters for the two-stage deformation and aging process of copper alloys, comprising six parameters in this study, includes a total of 313600 datasets. Identifying appropriate combinations of preparation parameters from this vast dataset is a challenging task that cannot be efficiently addressed through empirical trial-and-error alone. Therefore, a machine learning approach capable of accelerating the design of experiments is required. This study employs Bayesian optimization to address this challenge. Bayesian optimization offers numerous combinations of sample dataset construction methods and benchmark selection strategies for screening, which will be difficult to achieve solely through experimental validation with a large number of experiments. In this study, these parameters are optimized through function simulation, followed by screening a reasonable multi-objective utility function using experimental validation.

The study explores the impact of different basic sample dataset construction methods, benchmark selection methods, and multi-objective utility function construction methods on the iterative efficiency of Bayesian optimization. The results demonstrate that the combination of basic dataset construction and Bayesian optimization effectively addresses challenges such as the lack of alloy preparation parameter samples, providing a novel strategy for the efficient design of complex alloy preparation parameters.

Orthogonal experimental design provides a more balanced spatial distribution of data than random experimental design, crossover experimental design, and linear experimental design when acquiring the same amount of data. The data generated through orthogonal design exhibit less randomness and greater representativeness. Compared with the other three sample dataset construction methods, orthogonal design facilitates

the identification of the overall data trend and captures a broader information surface. Therefore, orthogonal experimental design is considered the most appropriate approach for data collection.

The static optimization benchmark selects the maximum value from the basic sample data as the benchmark. Throughout the iteration process, this benchmark focuses on optimizing based on existing information with a clear goal, but it has low explorability for newly acquired data. In contrast, the dynamic optimization benchmark selects the maximum value from both the basic sample data and the iteration data, maintaining high explorability throughout the process. The linear optimization benchmark begins with a smaller benchmark in the initial stages of iteration, offering higher utilizability, and gradually increases as the iterations progress, enhancing its explorability. Comparing the three benchmarks, it is evident that the linear optimization benchmark combines the high utilizability of the static optimization benchmark with the high explorability of the dynamic optimization benchmark. As a result, the linear optimization benchmark demonstrates superior iteration efficiency.

Using Bayesian optimization to design the preparation parameters enhances the efficiency of parameter design because the utility function integrates both the magnitude of the performance prediction value and the associated prediction uncertainty. This allows for the simultaneous optimization of the machine learning model and the performance itself [28,29]. The experimental validation and feedback iteration based on the preparation parameters recommended by the Bayesian optimization process complement the key data required to improve the model, thus contributing to the enhancement of the machine learning model's generalization ability. Therefore, this study designs various multi-objective utility functions based on the utility function.

Comparing the three multi-objective utility functions, the Bayesian optimization process based on the multi-objective utility function of E_{sqe} yields the best alloy performance, followed by E_{mu} and finally E_{me}. The multi-objective utility function E_{sqe} based on $\sqrt{Y_1^2+Y_2^2}$ is designed to balance the mechanical properties and EC of copper alloys. Through continuous iterative optimization, the final optimal performance obtained is the optimal performance under the balanced mechanical property and EC. While the E_{mu} and E_{me} multi-objective utility functions based on $|Y_1|\cdot|Y_2|$ and $Y_1\cdot Y_2$, respectively, also yield high-performance copper alloy preparation parameters, they focus more on the peak value of a single output compared to E_{sqe}, with less specificity towards data balance. Therefore, in this study, E_{sqe} is used as multi-objective utility function for optimizing mechanical and EC properties for copper alloy preparation design. It should be noted that the utility function calculation methods used in this paper are all aimed at the characteristics of the mutual constraint between the mechanical and electrical properties of copper alloys and the need for comprehensive performance improvement. When the performance relationship or design requirements change, the utility function in this paper may no longer be suitable.

In this study, the rapid design of copper alloy preparation parameters is achieved under the strategy combining basic dataset construction and Bayesian optimization, which consists of three core parameters, namely, orthogonal experimental design, linear optimization benchmark selection, and multi-objective utility function of E_{sqe}. Among them, the effectiveness of orthogonal design and linear optimization benchmark have been verified by Orowan precipitation strengthening equation, thus it has applicability in precipitation strengthening alloys; The multi-objective utility function of E_{sqe} is designed based on the mutual constraint between the mechanical and electrical properties of copper alloys and the demand for comprehensive performance improvement, and has been validated by the design of copper alloy process parameters. Therefore, the process design strategy proposed in this paper can be applied to alloy systems with similar strengthening methods and performance characteristics of copper alloys. By using this strategy, not only can we realize the rapid design of alloy preparation parameters with zero-sample, but also provide a solution for the autonomous intelligent experimental system of alloy material. By using the above strategy for fully active test point design and efficient selection iteration of optimization paths, it is expected that the rapid development of new material can be achieved through autonomous intelligent experiments.

4.2 Superiority of alloy performance after preparation parameters optimization

According to the results of Bayesian optimization iteration, it is determined that the preparation process of copper alloy specimens with optimal performance is as follows: 800 °C with 4 h homogenization → 67% deformation hot rolling at 800 °C (thickness from 30 mm to 10 mm) → 960 °C with 1 h solid solution treatment and water quenching → 60% deformation cold rolling (thickness from 10 mm to 4 mm) → 500 °C with 6 h aging treatment → 70% deformation cold rolling (thickness from 4 mm to 1.2 mm) → 425 °C with 6 h aging treatment. The tensile stress−strain curves of the alloy specimens after treatment by the above preparation process are shown in Fig. 7(a), and the measured UTS and EC are 878 MPa and 44.0%(IACS), respectively.

Figure 7(b) shows the comparison of the properties of copper alloys prepared in this study with the Cu−Ni−Si and Cu−Ni−Co−Si alloys reported in Refs. [3,24,30−38]. As can be seen from Fig. 7(b), the comprehensive performance of the alloys in this study is higher compared to those in the above-mentioned literature. In addition, compared with the commercial C70350 alloy with high Co content of 1.0−2.0 wt.%, the comprehensive performance of the alloy in this study reaches the level of C70350, while the Co content is only 0.7 wt.%, which is much lower than the lower limit of C70350 alloy.

The microstructure of the alloy after secondary aging is shown in Fig. 8. The results reveal the presence of a significant number of precipitated phases within the alloy, with the size of these precipitates approximately 10 nm. From the high resolution transmission electron microscope (HRTEM) observation of the precipitated phases shown in Figs. 8(b) and (c), it can be seen that the nano-precipitated phases are mainly $(Ni,Co)_2Si$ and Ni_3Si. The large number of diffusely precipitated phases pin dislocations on the one hand, resulting in an increase in the strength of the alloy, and on the other hand, the residual solid-solution alloying

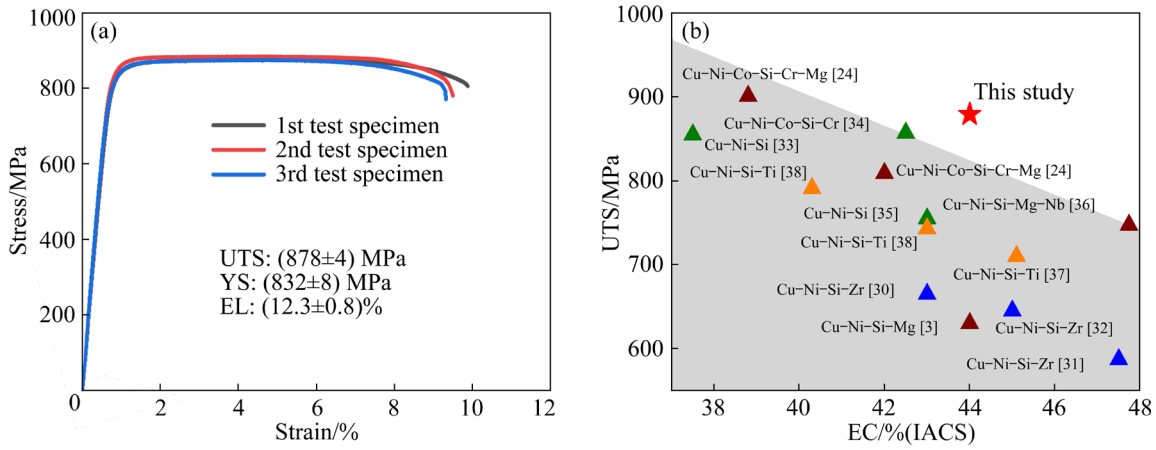

Fig. 7 Comparison of alloy properties: (a) Tensile stress−strain curves; (b) Comparison of alloy properties

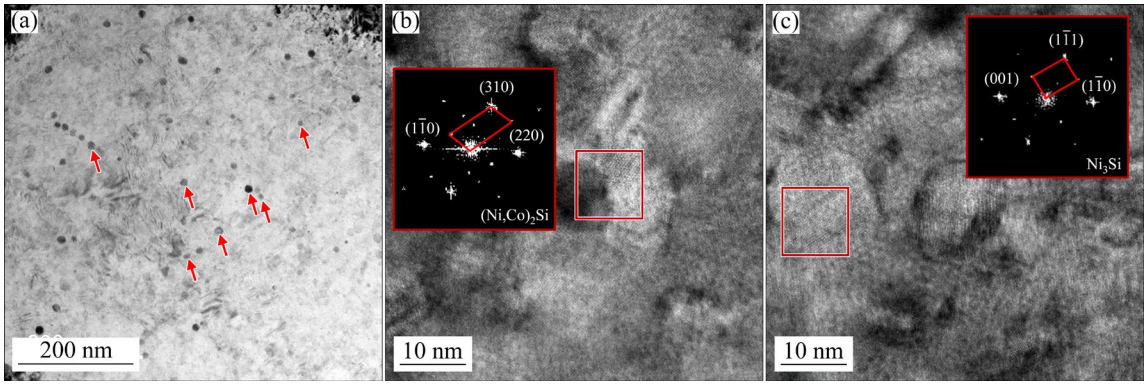

Fig. 8 TEM images of alloy specimen along [110] direction: (a) Bright-field TEM image; (b) HRTEM image of $(Ni,Co)_2Si$ precipitates; (c) HRTEM image of Ni_3Si precipitates

elements within the alloy matrix are reduced, which elevates the alloy EC.

4.3 Mechanisms influencing mechanical and electrical properties

The strengthening effect produced by the processing is a key factor affecting the mechanical properties of the alloys. After processing with optimized preparation parameters, a large number of grain boundaries, dislocations and nanoscale precipitation phases exist in the alloy, which cause the grain boundary strengthening, dislocation strengthening and precipitation strengthening on the matrix, respectively.

The grain boundary strengthening effect ($\Delta\sigma_G$) can be obtained using the Hall−Petch equation, as shown in Eq. (7) [39]:

$$\Delta\sigma_G=\frac{k}{\sqrt{d_G}} \tag{7}$$

where k is the coefficient, typically taken as 140 MPa·μm$^{1/2}$ [39], and d_G is the grain size.

The dislocation strengthening effect ($\Delta\sigma_d$) can be calculated from the dislocation density, as shown in Eq. (8) [40]:

$$\Delta\sigma_d=M\alpha Gb\rho^{1/2} \tag{8}$$

where α is a constant. Values of M, G, b, and α for copper alloys are 3.1, 48 GPa, 0.255 nm, and 0.2, respectively [41,42]. ρ represents the dislocation density, which is calculated from the micro-strain (ε) and the grain size d_G, as shown in Eq. (9) [43]:

$$\rho=\frac{2\sqrt{3}\varepsilon}{d_G b} \tag{9}$$

The micro-strain ε can be obtained through X-ray diffraction (XRD), as shown in Eq. (10):

$$\beta\cos\theta=\frac{k_2\lambda}{d_G}+4\varepsilon\sin\theta \tag{10}$$

where β is the half-width of the XRD diffraction peak, θ is the Bragg angle, λ is the radiation wavelength, and k_2 is a constant.

The XRD pattern and micro-strain of the alloy after processing with optimized preparation parameters are shown in Fig. 9. The fitted micro-strain is 0.1280, and the calculated dislocation strengthening effect is 236 MPa.

Figure 10 presents the inverse pole figure obtained from the electron backscattered diffraction

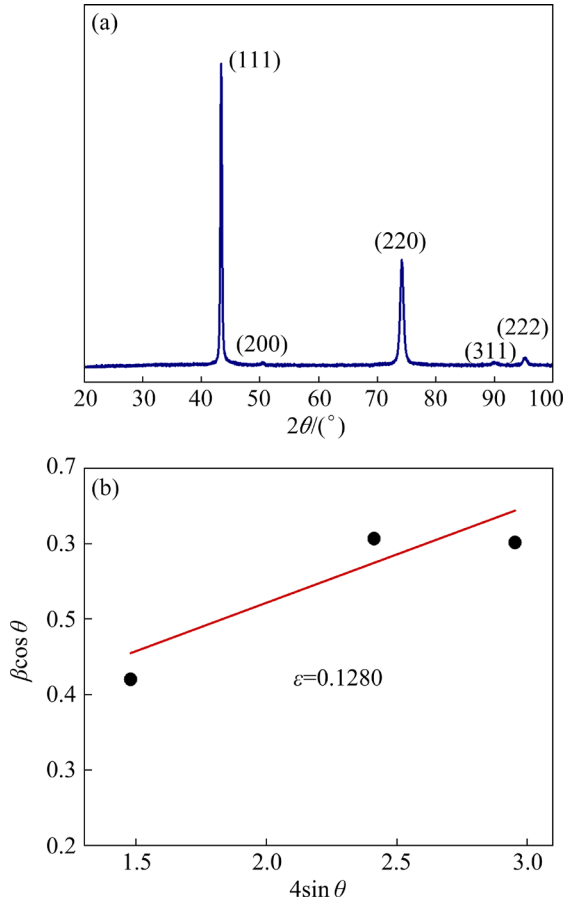

Fig. 9 XRD pattern and micro-strain of samples treated by optimized preparation parameters: (a) XRD pattern; (b) Micro-strain calculation

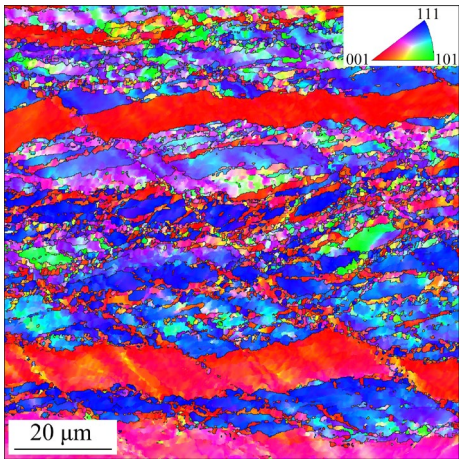

Fig. 10 Inverse pole figure of sample treated by optimized preparation parameters from EBSD

(EBSD). The average grain size is 1.8 μm, and the calculated grain boundary strengthening effect is 104 MPa. The precipitation strengthening effect primarily results from the interaction between dislocations and nano-sized precipitates, which can be described using the Orowan−Ashby equation, as

shown in Eq. (1). In this study, the Poisson ratio ν of the copper alloy is 0.34. The diameter and volume fraction of the precipitated phase are 10.2 nm and 0.03%, respectively, yielding a calculated precipitation strengthening effect of 413 MPa.

The effects of grain boundary strengthening, dislocation strengthening, and precipitation strengthening are shown in Table 5. After treatment with the optimized preparation parameters, the primary strengthening mechanism of the alloy is precipitation strengthening, with a strengthening effect of 413 MPa. This is followed by dislocation strengthening, which contributes a strengthening effect of 236 MPa. These results indicate that the preparation parameters optimized in this study primarily influence the dislocation strengthening and precipitation strengthening mechanisms.

Table 5 Calculated values of strengthening effects

d_G/μm	ε	ρ/m^{-2}	f_v/%
1.8	0.1280	9.66×10^{14}	0.03
d_p/nm	$\Delta\sigma_G$/MPa	$\Delta\sigma_d$/MPa	$\Delta\sigma_{Orowan}$/MPa
10.2	104	236	413

The decrease in the EC of the alloy is primarily attributed to the scattering of free electrons by solid-solution alloying elements, precipitated phases, dislocations, and grain boundaries. The alloy resistivity is calculated by Eq. (11):

$$\rho_{alloy}=\rho_0+\Delta\rho_p+\Delta\rho_d+\Delta\rho_G+\Delta\rho_s \quad (11)$$

where ρ_{alloy} is the resistivity of the alloy, ρ_0 is the resistivity of pure copper (1.72×10^{-8} Ω·m), $\Delta\rho_p$, $\Delta\rho_d$, $\Delta\rho_G$, and $\Delta\rho_s$ denote the increase in resistivity caused by precipitates, dislocations, grain boundaries, and solid-solution atoms, respectively.

Among them, the scattering of electrons by the precipitation phase is related to the precipitation phase spacing, and when the precipitation phase spacing is greater than the electron free range of pure copper (42 nm), the scattering effect on electrons is small. In this study, the precipitation phase spacing of the alloy is about 58 nm, and thus the effect of the precipitation phase on the EC is small and negligible.

The change in resistivity $\Delta\rho_d$ caused by electron scattering due to dislocations is represented by Eq. (12) [44]:

$$\Delta\rho_d=A_d\rho \quad (12)$$

where A_d is a constant, which is 2.7×10^{-25} Ω·m^3 for copper alloy.

The change in resistivity due to electron scattering by grain boundaries, $\Delta\rho_G$, is given by Eq. (13) [45]:

$$\Delta\rho_G=\frac{A_G}{d_G} \quad (13)$$

where A_G is a constant, which is 3.58×10^{-16} Ω·m^2 for copper alloys.

The total of increase in resistivity due to dislocations and grain boundaries in the alloy is calculated from Eq. (12) and Eq. (13) to be 2.61×10^{-10} Ω·m. Since the total resistivity of the alloy is 3.91×10^{-8} Ω·m, the increase in resistivity of the alloy due to the solid-solution elements is calculated to be 1.96×10^{-8} Ω·m, as shown in Table 6. Further, it is calculated that dislocations, grain boundaries, and solid-solution elements resulted in a decrease in the EC of the alloy by 0.7%(IACS), 0.5%(IACS), and 54.8%(IACS), respectively. Thus, the atoms of the alloying elements that are solidly dissolved in the matrix are the main factors affecting the EC.

Table 6 Calculated values of increase in resistivity

d_G/μm	ρ/m^{-2}	$\Delta\rho_d$/(Ω·m)	$\Delta\rho_G$/(Ω·m)	$\Delta\rho_s^*$/(Ω·m)
1.8	9.66×10^{14}	2.61×10^{-10}	1.99×10^{-9}	1.96×10^{-8}

$\Delta\rho_s^*$ is calculated as the difference between the total resistivity of the alloy and the sum of $\Delta\rho_d$ and $\Delta\rho_G$

5 Conclusions

(1) The effects of basic sample dataset construction, optimization benchmarks, and multi-objective utility functions on design efficiency were investigated through a combination of function simulation and alloy experiment. It is found that the combination of orthogonal design, linear benchmark, and shifted multiplicative utility function achieves the highest optimization efficiency and the best optimization performance.

(2) The proposed strategy was applied to the experimental iteration of a new Cu−Ni−Co−Si alloy with an ultra-low Co content (0.7 wt.% Co). The rapid design of a two-stage deformation and aging process, involving six preparation parameters, was achieved for this zero-sample alloy through a total of only 23 experiments.

(3) Under the designed preparation condition,

the measured UTS and EC of the new Cu−Ni−Co−Si alloy with ultra-low Co content are 878 MPa and 44.0%(IACS), respectively, which reach the comprehensive performance levels of the Cu−Ni−Co−Si alloy (C70350 alloy) containing 1.0−2.0 wt.% Co.

CRediT authorship contribution statement

Hui-qiang MA: Data curation, Investigation, Writing − Original draft; **Hong-tao ZHANG:** Investigation, Conceptualization, Methodology, Writing − Review & editing; **Hua-dong FU:** Investigation, Writing − Review & editing; **Jing-tai SUN:** Investigation, Writing − Review & editing; **Jian-xin XIE:** Conceptualization, Resources, Writing − Review & editing.

Declaration of competing interest

The authors declare that they have no known competing financial interests or personal relationships that could have appeared to influence the work reported in this paper.

Acknowledgments

This work was supported by the National Natural Science Foundation of China (Nos. 52404387, 52090041, 52374379, 52425409), Xiaomi Young Scholars Program, China, the National Postdoctoral Program for Innovative Talents, China (No. BX20230042), and China Post-doctoral Science Foundation (No. 2024M750174).

References

[1] YANG Hai-te, WANG Wen-wei-jiao, WANG Chen, WANG Jian, ZHOU Jian-hui, TONG Chang-qing, CHEN Jun-feng, WANG Bing-shu. Effects of aging process on properties and precipitation kinetics of Cu−Cr−Zr alloy strips [J]. Transactions of Nonferrous Metals Society of China, 2023, 33: 2439−2448.

[2] SHEN Ke-chang, GONG Qing-tao, SUN Zhong-yu, SUN Hong-tu, MA Bin-jie, WANG Wei-min. Damage characteristics of Cu−Cr−Zr alloy rail of electromagnetic railgun after simulated launch[J]. Transactions of Nonferrous Metals Society of China, 2024, 34: 2589−2604.

[3] MONZEN R, WATANABE C. Microstructure and mechanical properties of Cu−Ni−Si alloys [J]. Materials Science and Engineering: A, 2008, 483/484: 117−119.

[4] LEI Qian, LI Zhou, DAI Ce, WANG Jin-san, CHEN Xi, XIE Jie-min, YANG Wen-wei, CHEN Ding-long. Effect of aluminum on microstructure and property of Cu−Ni−Si alloys [J]. Materials Science and Engineering: A, 2013, 572: 65−74.

[5] JIA Yan-lin, PANG Yong, YI Jiang, LEI Qian, LI Zhou, XIAO Zhu. Effects of pre-aging on microstructure and properties of Cu−Ni−Si alloys [J]. Journal of Alloys and Compounds, 2023, 942: 169033.

[6] HU Ting, CHEN Jiang-hua, LIU Ji-zi, LIU Zi-ran, WU Cui-lan. The crystallographic and morphological evolution of the strengthening precipitates in Cu−Ni−Si alloys [J]. Acta Materialia, 2013, 61: 1210−1219.

[7] LEI Qian, LI Zhou, GAO Yang, PENG Xi, DERBY B. Microstructure and mechanical properties of a high strength Cu−Ni−Si alloy treated by combined aging processes [J]. Journal of Alloys and Compounds, 2017, 695: 2413−2423.

[8] XIE Jian-xin. Prospects of materials genome engineering frontiers[J]. Materials Genome Engineering Advances, 2023, 1: e17.

[9] LI Cong, WANG Xian-hui, LI Bo, SHI Jing, LIU Yan-feng, XIAO peng. Effect of cold rolling and aging treatment on the microstructure and properties of Cu−3Ti−2Mg alloy [J]. Journal of Alloys and Compounds, 2020, 818: 152915.

[10] LIU Kun, CHEN Xi-zhang, SHEN Qing-kai, PAN Zeng-xi, SINGH R A, JAYALAKSHMI S, KONOVALOV S. Microstructural evolution and mechanical properties of deep cryogenic treated Cu−Al−Si alloy fabricated by Cold Metal Transfer (CMT) process [J]. Materials Characterization, 2020, 159: 110011.

[11] XIE Jian-xin, SU Yan-jing, ZHANG Da-wei, FENG Qiang. A vision of materials genome engineering in China [J]. Engineering, 2022, 10: 10−12.

[12] LIU Yue, ZHAO Tian-lu, JU Wang-wei, SHI Si-qi. Materials discovery and design using machine learning [J]. Journal of Materiomics, 2017, 3: 159−177.

[13] JUAN Yong-fei, NIU Guo-shuai, YANG Yang, XU Zi-han, YANG Jian, TANG Wen-qi, JIANG Hai-tao, HAN Yan-feng, DAI Yong-bing, ZHANG Jiao, SUN Bao-de. Accelerated design of Al−Zn−Mg−Cu alloys via machine learning [J]. Transactions of Nonferrous Metals Society of China, 2024, 34: 709−723.

[14] LI Xin, SHAN Guang-cun, ZHAO Hong-bin, SHEK C H. Domain knowledge aided machine learning method for properties prediction of soft magnetic metallic glasses [J]. Transactions of Nonferrous Metals Society of China, 2023, 33: 209−219.

[15] XU Peng-cheng, JI Xiao-bo, LI Min-jie, LU Wen-cong. Small data machine learning in materials science [J]. npj Computational Materials, 2023, 9: 42.

[16] NGUYEN D S, PARK H S, LEE C M. Optimization of selective laser melting process parameters for Ti−6Al−4V alloy manufacturing using deep learning [J]. Journal of Manufacturing Processes, 2020, 55: 230−235.

[17] TAMURA R, OSADA T, MINAGAWA K, KOHATA T, HIROSAWA M, TSUDA K, KAWAGISHI K. Machine learning-driven optimization in powder manufacturing of Ni−Co based superalloy [J]. Materials & Design, 2021, 198: 109290.

[18] CHEN Yi-fei, TIAN Yuan, ZHOU Yu-mei, FANG Da-qing, DING Xiang-dong, SUN Jun, XUE De-zhen. Machine learning assisted multi-objective optimization for materials processing parameters: A case study in Mg alloy [J]. Journal of Alloys and Compounds, 2020, 844: 156159.

[19] ZHANG Hong-tao, FU Hua-dong, SHEN Yu-heng, XIE Jian-xin. Rapid design of secondary deformation-aging parameters for ultra-low Co content Cu−Ni−Co−Si−X alloy via Bayesian optimization machine learning [J]. International Journal of Minerals, Metallurgy and Materials, 2022, 29: 1197−1205.

[20] MABUCHI M, HIGASHI K. Strengthening mechanisms of Mg−Si alloys [J]. Acta Materialia, 1996, 44: 4611−4618.

[21] LEI Qian, LI Zhou, ZHU An-yin, QIU Wen-ting, LIANG Shu-quan. The transformation behavior of Cu−8.0Ni−1.8Si−0.6Sn−0.15Mg alloy during isothermal heat treatment [J]. Materials Characterization, 2011, 62, 904−911.

[22] ZHANG Hong-tao, FU Hua-dong, ZHU Shuai-cheng, YONG Wei, XIE Jian-xin. Machine learning assisted composition effective design for precipitation strengthened copper alloys [J]. Acta Materialia, 2021, 215: 117118.

[23] XU Liu-liu, FAN Ding-qiang, LIU Kang-ning, XU Wang-yang, YU Rui. A machine learning framework for intelligent development of ultra-high performance concrete (UHPC): From dataset cleaning to performance predicting [J]. Expert Systems with Applications, 2024, 242: 122790.

[24] MA Mu-zhi, LI Zhou, XIAO Zhu, JIA Yan-lin, MENG Xiang-peng, JIANG Yan-bin, HU Yue. Microstructure and properties of Cu−Ni−Co−Si−Cr−Mg alloys with different Si contents after multi-step thermo-mechanical treatment [J]. Materials Science and Engineering: A, 2022, 850: 143532.

[25] ZHAO Zhi-lei, XIAO Zhu, LI Zhou, QIU Wen-ting, JIANG Hong-yun, LEI Qian, LIU Ze-ru, JIANG Yan-bin, ZHANG Sang-jiang. Microstructure and properties of a Cu−Ni−Si−Co−Cr alloy with high strength and high conductivity [J]. Materials Science and Engineering: A, 2019, 759: 396−403.

[26] XUE De-zhen, BALACHANDRAN P V, HOGDEN J, THEILER J, XUE De-qing, LOOKMAN T. Accelerated search for materials with targeted properties by adaptive design [J]. Nature Communications, 2016, 7: 11241.

[27] XUE De-zhen, XUE De-qing, YUAN Rui-hao, ZHOU Yu-mei, BALACHANDRAN P V, DING Xiang-dong, SUN Jun, LOOKMAN T. An informatics approach to transformation temperatures of NiTi-based shape memory alloys [J]. Acta Materialia, 2017, 125: 532−541.

[28] BALACHANDRAN P V, XUE De-zhen, THEILER J, HOGDEN J, LOOKMAN T. Adaptive strategies for materials design using uncertainties [J]. Scientific Reports, 2016, 6: 19660.

[29] LOOKMAN T, BALACHANDRAN P V, XUE De-zhen, HOGDEN J, THEILER J. Statistical inference and adaptive design for materials discovery [J]. Current Opinion in Solid State and Materials Science, 2017, 21: 121−128.

[30] XIAO Xiang-peng, XIONG Bai-qing, WANG Qiang-song, XIE Guo-liang, PENG Li-jun, HUANG Guo-xing. Microstructure and properties of Cu−Ni−Si−Zr alloy after thermomechanical treatments [J]. Rare Metals, 2013, 32: 144−149.

[31] WANG Wei, KANG Hui-jun, CHEN Zong-ning, CHEN Zhong-jun, ZOU Cun-lei, LI Ren-geng, YIN Guo-mao, WANG Tong-min. Effects of Cr and Zr additions on microstructure and properties of Cu−Ni−Si alloys [J]. Materials Science and Engineering: A, 2016, 673: 378−390.

[32] CHENNA KRISHNA S, SRINATH J, JHA A K, PANT B, SHARMA S C, GEORGE K M. Microstructure and properties of a high-strength Cu−Ni−Si−Co−Zr alloy [J]. Journal of Materials Engineering and Performance, 2013, 22: 2115−2120.

[33] LI Jiang, HUANG Guo-jie, MI Xu-jun, PENG Li-jun, XIE Hao-feng, KANG Yong-lin. Effect of Ni/Si mass ratio and thermomechanical treatment on the microstructure and properties of Cu−Ni−Si Alloys [J]. Materials, 2019, 12: 2076.

[34] BAN Yi-jie, GENG Yong-feng, HOU Jin-rui, ZHANG Yi, ZHOU Meng, JIA Yan-lin, TIAN Bao-hong, LIU Yong, LI Xu, VOLINSKY A A. Properties and precipitates of the high strength and electrical conductivity Cu−Ni−Co−Si−Cr alloy [J]. Journal of Materials Science & Technology, 2021, 93: 1−6.

[35] LEE E, HAN S, EUH K, LIM S, KIM S. Effect of Ti addition on tensile properties of Cu−Ni−Si alloys [J]. Metals and Materials International, 2011, 17: 569−576.

[36] WANG Wen-wei-jiao, WANG Jian, LI Shang-jin, WANG Chen, ZHOU Jian-hui, ZENG Jia-wei, TAN Wen-long, WANG Bing-shu. Effects of Nb addition on the properties and microstructure of Cu−Ni−Si−Mg alloy [J]. Materials Characterization, 2022, 194: 112451.

[37] WATANABE C, TAKESHITA S, MONZEN R. Effects of small addition of Ti on strength and microstructure of a Cu−Ni−Si alloy [J]. Metallurgical and Materials Transactions A, 2015, 46: 2469−2475.

[38] LEE E, EUH K, HAN S Z, LIM S, LEE J, KIM S. Tensile and electrical properties of direct aged Cu−Ni−Si−*x*%Ti alloys [J]. Metals and Materials International, 2013, 19: 183−188.

[39] HANSEN N. Hall−Petch relation and boundary strengthening [J]. Scripta Materialia, 2004, 51: 801−806.

[40] BALOGH L, UNGÁR T, ZHAO Yong-hao, ZHU Yun-tian, HORITA Z, XU Cheng, LANGDON T G. Influence of stacking-fault energy on microstructural characteristics of ultrafine-grain copper and copper−zinc alloys [J]. Acta Materialia, 2008, 56: 809−820.

[41] AG D. Precipitation-hardening of metals [J]. British Dental Journal, 1951, 90: 205−211.

[42] PAGARE G, JAIN E, SANYAL S P. Density functional investigation on electronic structure and elastic properties of BeX at high pressure [J]. Indian Journal of Physics, 2016, 90: 271−281.

[43] GHOLAMI M, VESELY J, ALTENBERGER I, KUHN H A, JANECEK M, WOLLMANN M, WAGNER L. Effects of microstructure on mechanical properties of CuNiSi alloys [J]. Journal of Alloys and Compounds, 2017, 696: 201−212.

[44] DEY S, SULTANA N, KAISER M S, DEY P, DATTA S. Computational intelligence based design of age-hardenable aluminium alloys for different temperature regimes [J]. Materials & Design, 2016, 92: 522−534.

[45] MANNAN K M, KARIM K R. Grain boundary contribution to the electrical conductivity of polycrystalline Cu films [J]. Journal of Physics F: Metal Physics, 1975, 5: 1687−1693.

一种针对零样本复杂合金制备参数快速设计的机器学习策略

马慧强[1]，张洪涛[1,2,3]，付华栋[1,2,3,4]，孙竟泰[1]，谢建新[1,2,3,4]

1. 北京科技大学 北京材料基因工程高精尖创新中心，北京 100083；
2. 北京科技大学 材料先进制备技术教育部重点实验室，北京 100083；
3. 北京科技大学 现代交通金属材料与加工技术北京实验室，北京 100083；
4. 辽宁材料实验室 材料智能技术研究所，沈阳 110004

摘　要：为了应对新开发合金在制备参数设计中面临的零样本问题，提出了一种结合基本数据集构建和贝叶斯优化的机器学习新策略。研究了基本样本数据集构建方法、优化基准点和多目标效能函数对贝叶斯优化效果的影响，发现正交试验设计、线性基准点和的组合具有最佳的优化效果。将该方法应用于作者课题组前期设计的超低 Co 含量 (0.7% Co，质量分数) 新型 Cu−Ni−Co−Si 合金，仅用 23 次实验实现了零样本新合金的两级形变−时效共 6 个制备参数的快速优化设计。新合金的实测极限抗拉强度和电导率分别为 878 MPa 和 44.0%(IACS)，达到了含 1.0%~2.0% Co (质量分数) Cu−Ni−Co−Si 合金 (C70350 合金) 的综合性能水平。

关键词：Cu−Ni−Co−Si 合金；制备参数；机器学习；贝叶斯优化

(Edited by Wei-ping CHEN)